

Plastic flow in polycrystal states in a binary mixture

Toshiyuki Hamanaka and Akira Onuki

Department of Physics, Kyoto University, Kyoto 606-8502, Japan

(Dated: February 1, 2008)

Using molecular dynamics simulation we examine dynamics in sheared polycrystal states in a binary mixture containing 10% larger particles in two dimensions. We find large stress fluctuations arising from sliding motions of the particles at the grain boundaries, which occur cooperatively to release the elastic energy stored. These dynamic processes are visualized with the aid of a sixfold angle $\alpha_j(t)$ representing the local crystal orientation and a disorder variable $D_j(t)$ representing a deviation from the hexagonal order for particle j .

PACS numbers: 62.20.Fe, 61.82.Rx, 61.43.-j

Understanding the deformation mechanisms of polycrystals under applied strain is of great scientific and technological importance in materials science [1, 2, 3, 4]. If the typical grain size exceeds a critical size $d_c \sim 10\text{nm}$, interplay of grain boundaries and dislocation motions determines the mechanical properties. For very small grain sizes less than d_c , some simulations suggested that plastic deformations are caused by sliding motions at the grain boundaries. There remain a number of puzzles in polycrystal rheology not yet simulated microscopically, such as the Portevin-Le Chatelier effect in dilute alloys caused by intermittent yielding [5]. On the other hand, in physics, dynamics of sheared glassy materials has been studied extensively [6, 7], including microscopic particle systems [8, 9, 10], granular materials [11, 12], and foams [13], while not enough attention has been paid to polycrystal rheology.

Recently, using molecular dynamics simulation, we have examined the dynamics of polycrystal states realized on very small scales in a model binary mixture [14]. The parameters we have changed are the size ratio of the diameters of the two components σ_2/σ_1 , the temperature T , and the composition c . Polycrystal states appear as intermediate states between crystal and glass, where the grain boundary motions are severely slowed down with size dispersity. The particles in the grain boundary regions have a relatively high mobility leading to dynamic heterogeneity on long time scales. Thus investigating the jamming dynamics over wide ranges of σ_2/σ_1 and c helps us to understand the glass dynamics as highly frustrated limits. In this paper, we will present simulation results on polycrystal rheology, however, at fixed σ_2/σ_1 and c .

Our two-dimensional (2D) system is composed of the bulk region with volume $V = L^2$ and the top and bottom boundary regions with volume $0.1V$, as can be seen in Fig. 1. Shear flow was realized by the relative boundary motion of the boundaries, where the top and bottom velocities are $\pm\dot{\gamma}L/2$, with $\dot{\gamma}$ being an applied shear rate. In the bulk region, $0 < x, y < L$, a mixture of large and small particles interact via a truncated Lenard-Jones potential of the form, $v_{\alpha\beta}(r) = 4\epsilon[(\sigma_{\alpha\beta}/r)^{12} - (\sigma_{\alpha\beta}/r)^6] - C_{\alpha\beta}$ ($\alpha, \beta = 1, 2$), characterized by the energy ϵ and the

soft-core diameter $\sigma_{\alpha\beta} = (\sigma_\alpha + \sigma_\beta)/2$ with $\sigma_2/\sigma_1 = 1.4$. For $r > r_{\text{cut}} = 3.2\sigma_1$, we set $v_{\alpha\beta}(r) = 0$ and the constant $C_{\alpha\beta}$ ensures the continuity of $v_{\alpha\beta}(r)$ at the cut-off $r = r_{\text{cut}}$. In this paper, the particle numbers are fixed at $N_1 = 900$ and $N_2 = 100$ or $c = N_2/(N_1 + N_2) = 0.1$ in the bulk. The volume V is chosen such that the volume fraction of the soft-core regions is fixed at 1 or at $\phi = (N_1\sigma_1^2 + N_2\sigma_2^2)/V = 1$, so $L = 33.1\sigma_1$. To each boundary ($-0.1L < y < 0$ or $L < y < 1.1L$), 100 small particles with radius σ_1 are attached by the spring potential $10\epsilon|\mathbf{r} - \mathbf{R}_j|^2$. They also interact with the other particles in the boundary and bulk regions with the common Lenard-Jones potential. Before our simulation, the attached positions \mathbf{R}_j ($j = 1, \dots, 100$) in each boundary wall were determined in a liquid state realized at $T = 2\epsilon/k_B$ with the Lenard-Jones potential only.

We integrated the Newton equations using the leapfrog algorithm [15] under the periodic boundary condition in the horizontal (y) direction, with the mass ratio being $m_1/m_2 = (\sigma_1/\sigma_2)^2$. The time step of integration is 0.002τ with

$$\tau = \sigma_1 \sqrt{m_1/\epsilon}. \quad (1)$$

We will measure the time t in units of τ and the shear rate $\dot{\gamma}$ in units of τ^{-1} . Without shear ($\dot{\gamma} = 0$), (i) we first equilibrated the system in a liquid state at $T = 2\epsilon/k_B$ in a time interval of 10^3 and then quenched it to the final temperature $T = 0.2\epsilon/k_B$. (ii) After a relaxation time of 5×10^3 , there was no appreciable time evolution in various quantities obtained as an average over the particles (see Fig.7 of Ref.[14]). (iii) After these steps, we applied a constant shear to the system.

Since a large fraction of the particles are enclosed by six particles in 2D dense particle systems, the local crystalline order is represented by the sixfold orientation [16]. We define the orientation angle α_j in the range $[0, \pi/3]$ for each particle j using the following complex number,

$$\Psi_j = \sum_{k \in \text{bonded}} \exp[6i\theta_{jk}] = |\Psi_j|e^{6i\alpha_j}, \quad (2)$$

where the summation is over the particles "bonded" to the particle j . The two particles $j \in \alpha$ and $k \in \beta$ are

bonded, if their distance $|\mathbf{r}_j - \mathbf{r}_k|$ is shorter than $R_{\alpha\beta} = 1.25\sigma_{\alpha\beta}$ [8]. The upper cut-off $R_{\alpha\beta}$ is slightly longer than the first peak position of the pair-correlation function $g_{\alpha\beta}(r)$. The θ_{jk} is the angle of the relative vector $\mathbf{r}_j - \mathbf{r}_k$ with respect to the x axis. Next we construct another nonnegative-definite variable representing the degree of disorder for each particle j by [14]

$$D_j = 2 \sum_{k \in \text{bonded}} [1 - \cos 6(\alpha_j - \alpha_k)]. \quad (3)$$

For a perfect crystal at low T this quantity arises from the thermal vibrations and is nearly zero, but for particles around defects it assumes large values in the range 5–20.

In Fig. 1, we show the particle configuration with the large particles in blue, the angles α_j , and the disorder variable D_j for sheared states with (a) $\dot{\gamma} = 10^{-4}$, (b) 10^{-3} , and (c) 10^{-2} . See Ref.[14] for the color map of α_j and Fig.3 below for that of D_j . The polycrystal grains and the grain boundaries are unambiguously visualized using α_j and D_j . By comparing the three kinds of snapshots for each state, we notice that the large particles

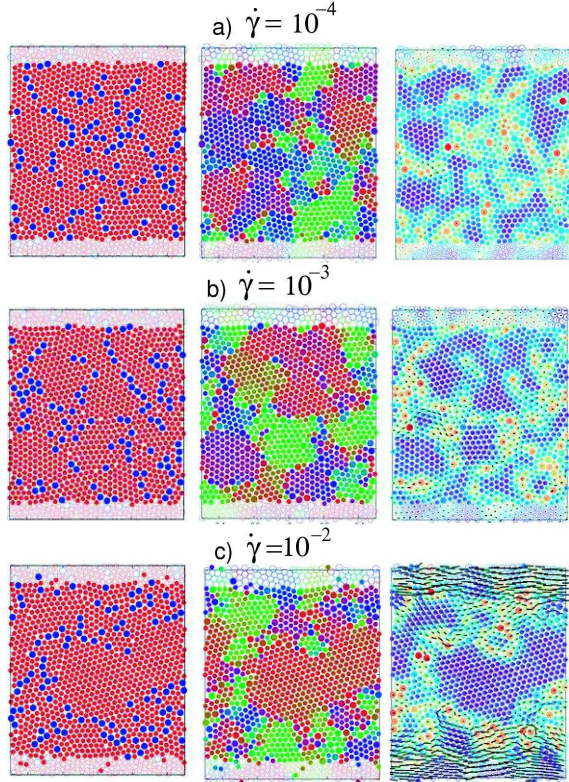


FIG. 1: (Color on line) Particle configuration (left), sixfold orientation order (middle), and disorder variable (right) for three sheared states, where $\dot{\gamma} = 10^{-4}$ (top), 10^{-3} (middle), and 10^{-2} (bottom), in a binary mixture with $c = 0.1$ and $\sigma_2/\sigma_1 = 1.4$. The snapshots for $\dot{\gamma} = 10^{-4}$ and 10^{-3} are very similar, while for $\dot{\gamma} = 10^{-2}$ the displacement vectors of the particles in a time interval of 10 (right) show shear localization near the boundaries.

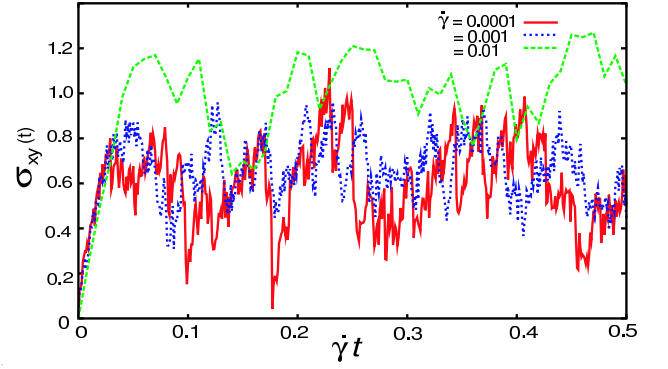


FIG. 2: (Color on line) Shear stress $\sigma_{xy}(t)$ vs strain $\dot{\gamma}t$ after application of shear in units of $\epsilon\sigma_1^{-2}$ with $\dot{\gamma} = 10^{-4}$, 10^{-3} , and 10^{-2} , exhibiting large temporal fluctuations and strong shear thinning.

tend to form the grain boundaries. This tendency can be seen even without shear [14], but is intensified under shear. Remarkably, the grain structures are insensitive to $\dot{\gamma}$ for not very large shear ($\dot{\gamma} \lesssim 10^{-3}$ here), where the effect of the boundary walls does not extend into the bulk and the time-average of the horizontal velocity is linear with the gradient $\dot{\gamma}$. To support this weakness of the boundary effect, almost the same grain structures were realized under the Lee-Edwards boundary condition [15] (not shown in this paper). However, for very large shear $\dot{\gamma} = 10^{-2}$ in (c), the velocity gradient becomes localized near the boundaries with larger crystalline regions in the middle being continuously rotated and deformed.

In Fig. 2, the average shear stress $\sigma_{xy}(t)$ is displayed in units of $\epsilon\sigma_1^{-2}$ as a function of the average strain $\dot{\gamma}t$ after application of shear at $t = 0$, which is the sum of the microscopic shear-stress contributions over all the particles in the bulk divided by V [7, 15]. Each curve is a result of a single simulation run. It undergoes large temporal fluctuations, arising from plastic deformations of the polycrystal structures. For not large shear, it varies from a minimum about 0.4 to a maximum about 1.0 on a time scale of order $0.1\dot{\gamma}^{-1}$, and its time-average is insensitive to $\dot{\gamma}$. The effective viscosity η_{eff} (time-average of $\sigma_{xy}/\dot{\gamma}$) thus behaves as $\dot{\gamma}^{-1}$. At the largest shear $\dot{\gamma} = 10^{-2}$, the time scale of the fluctuations is longer than $0.1\dot{\gamma}^{-1}$ and $\sigma_{xy}(t)$ is larger than in the lower shear cases.

In Fig. 3, we display $D_j(t)$ at (a) $t = 1110$, (b) 1120, and (c) 1130 at $\dot{\gamma} = 10^{-3}$, superimposing the displacement vectors $\Delta\mathbf{r}_j(t) = \mathbf{r}_j(t + \Delta t) - \mathbf{r}_j(t)$ with $\Delta t = 10$. The color is given to each picture independently, according to its minimum and maximum of D_j . We also present $\sigma_{xy}(t)$ in the corresponding time range. Between $t = 1110$ and 1120, the deformations are mostly “elastic” as in (a) and $\sigma_{xy}(t)$ gradually increases on the average. However, between $t = 1120$ and 1130, the picture (b) indicates significant “sliding” particle motions in the grain boundary regions, which are of order σ_1 even for this

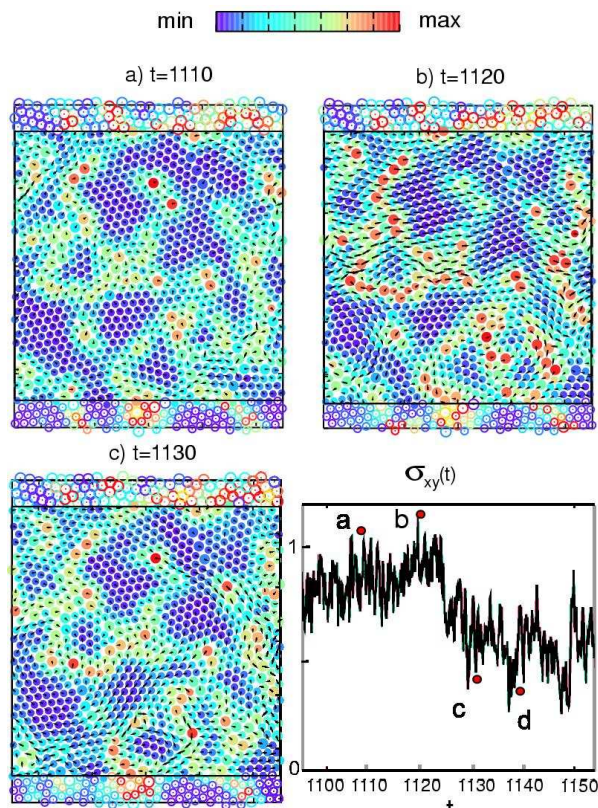


FIG. 3: (Color on line) Disorder variable D_j at (a) $t = 1110$, (b) 1120, and (c) 1130 at $\dot{\gamma} = 10^{-3}$. The arrows represent the particle displacement $\Delta \mathbf{r}_j$ in the subsequent time interval of width 10, which are large in (b) for the particles in the grain boundary regions. The average stress $\sigma_{xy}(t)$ is also shown in this time region.

small Δt . These sliding motions are triggered collectively throughout the system (in our small system), leading to a catastrophic drop of $\sigma_{xy}(t)$. The particles written in orange, which are mostly larger ones, may be regarded to be in disordered configurations. Their number is of order 10 in (a) and (c), while it is about 50 in (b). In (c) noticeable particle displacements still continue. Large scale collective motions of the particles within the grains are also conspicuous, which was already noticed in our previous simulation without shear [14].

In summary, in polycrystal states with very small grains, we have found intermittent yielding on a time scale of $0.1\dot{\gamma}^{-1}$ for not very large $\dot{\gamma}$. It is caused by cooperative sliding motions in the grain boundary regions in agreement with the atomistic simulations [1, 2, 3, 4]. In our small-scale simulation, however, we cannot determine the spatial scale of the cooperative sliding extending over grains, which should be relevant in real systems. With increasing c , the typical sizes of the crystalline regions

become smaller and the stress fluctuations gradually decrease. That is, weaker disorder results in larger stress fluctuations in plastic flow. The proportionality of the structural relaxation time to $\dot{\gamma}^{-1}$ and the shear thinning behavior $\eta_{\text{eff}} \propto \dot{\gamma}^{-1}$ still hold for glasses, as observed experimentally [17] and numerically [8]. Similar plastic flow phenomena should be observable in colloidal mixtures on expanded scales, as a future experimental system. It is of great interest how our findings can be related to the other well-known examples of enhanced stress fluctuations, where the effect of the size dispersity should be further examined [5, 11, 12, 13].

This work was supported by Grants in Aid for Scientific Research and for the 21st Century COE project (Center for Diversity and Universality in Physics) from the Ministry of Education, Culture, Sports, Science and Technology of Japan.

-
- [1] J. Schiotz, F.D. Di Tolla, and K.W. Jacobsen, *Nature* **391**, 561 (1998).
 - [2] A. Hasnaoui, H. Van Swygenhoven, and P.M. Derlet, *Phys. Rev. B* **66**, 184112 (2002).
 - [3] S. Yip, *Nature Mater.* **3**, 11 (2004).
 - [4] V. Yamakov, D. Wolf, S. R. Phillpot, A. K. Mukherjee, and H. Gleiter, *Nature Materials* **3**, 43 (2004).
 - [5] Y. Estrin and L.P. Kubin, *Mater. Sci. Eng., A* **137**, 125 (1991); G. D'Anna and F. Nori, *Phys. Rev. Lett.* **85**, 4096 (2000); P. Barat, A. Sarkar, P. Mukherjee, and S.K. Bandyopadhyay, *Phys. Rev. Lett.* **94**, 055502 (2005).
 - [6] A.J. Liu and S.R. Nagel, *Nature* **396**, 21 (1998).
 - [7] A. Onuki, *Phase Transition Dynamics* (Cambridge University Press, Cambridge, 2002).
 - [8] R. Yamamoto and A. Onuki, *J. Phys. Soc. Jpn.*, **66** 2545 (1997); *Phys. Rev. E* **58**, 3515 (1998).
 - [9] M. Fuchs, M. E. Cates: *Phys. Rev. Lett.* **89**, 248304 (2002); K. Miyazaki, D.R. Reichman, *Phys. Rev. E* **66**, 050501 (R) (2002).
 - [10] F. Varnik, L. Bocquet, and J.L. Barrat, *J. Chem. Phys.* **120**, 2788 (2004).
 - [11] B. Miller, C.O'Hern and R.P. Behringer, *Phys. Rev. Lett.* **77**, 3110 (1996).
 - [12] O.J. Schwarz, Y. Horie, and M. Shearer, *Phys. Rev. E* **57**, 2053 (1998).
 - [13] T. Okuzono and K. Kawasaki, *Phys. Rev. E*, **51**, 1246 (1995).
 - [14] T. Hamanaka and A. Onuki, *Phys. Rev. E* **74**, 011506 (2006); *Phys. Rev. E* **75**, 041503 (2007).
 - [15] J.P. Hansen and I.R. McDonald, *Theory of Simple Liquids*, (Academic Press, London, 1986).
 - [16] B.I. Halperin and D. R. Nelson, *Phys. Rev. Lett.* **41**, 121 (1978).
 - [17] J.H. Simmons, R.K. Mohr, C.J. Montrose: *J. Appl. Phys.* **53**, 4075 (1982).